Journal of Biomolecular NMR (2005) 31: 35–47

Efficient and precise measurement of H^{α}–C^{α}, C^{α}–C', C^{α}–C^{β} and H^{N}–N residual dipolar couplings from 2D H^{N}–N correlation spectra

Robert L. McFeeters, C. Andrew Fowler, Vadim V. Gaponenko & R. Andrew Byrd*
Macromolecular NMR Section, Structural Biophysics Laboratory, National Cancer Institute, Frederick, MD 21702, U.S.A.

Received 9 August 2004; Accepted 18 October 2004

Key words: J-coupling, J-modulation, residual dipolar coupling, semi-constant time

Abstract

A suite of experiments are presented for the measurement of H^{α}–C^{α}, C^{α}–C', C^{α}–C^{β} and H^{N}–N couplings from uniformly ^{15}N, ^{13}C labeled proteins. Couplings are obtained from a series of intensity modulated two-dimensional H^{N}–N spectra equivalent to the common ^{1}H–^{15}N–HSQC spectra, alleviating many overlap and assignment issues associated with other techniques. To illustrate the efficiency of this method, H^{α}–C^{α}, C^{α}–C', and H^{N}–N isotropic scalar couplings were determined for ubiquitin from data collected in less than 4.5 h, C^{α}–C^{β} data collection required 10 h. The resulting couplings were measured with an average error of ± 0.06, ± 0.05, ± 0.04 and ± 0.10 Hz, respectively. This study also shows H^{α}–C^{α} and C^{α}–C^{β} couplings, valuable because they provide orientation of bond vectors outside the peptide plane, can be measured in a uniform and precise way. Superior accuracy and precision to existing 3D measurements for C^{α}–C' couplings and increased precision compared to IPAP measurements for H^{N}–N couplings are demonstrated. Minor modifications allow for acquisition of modulated H^{N}–C' 2D spectra, which can yield additional well resolved peaks and significantly increase the number of measured RDCs for proteins with crowded ^{1}H–^{15}N resonances.

Abbreviations: RDC – residual dipolar couplings; IPAP – in-phase, anti-phase; PAS – principal axis system.

Introduction

Residual dipolar couplings (RDCs) have become an important tool for studying biological macromolecules. By relating the orientation of bond vectors to a fixed molecular coordinate system achieved through weak alignment, RDCs provide global, long-range structural information complementary to local, short-range information traditionally based on torsion angles and NOE-derived distances. RDCs are highly effective restraints for improving solution structure calculations, validating existing structures, orienting domains, and providing new insight into dynamic processes on previously unattainable timescales (Tolman et al., 1995, 2001; Tjandra et al., 1997; Fischer et al., 1999; Evenas et al., 2001; Goto et al., 2001; Gaponenko et al., 2002; Peti et al., 2002; C.A. Fowler, submitted). To effectively utilize the wealth of available information, it is necessary to measure as many couplings as possible with the highest accuracy. Measurement of multiple RDCs for a given peptide plane provides complimentary long-range information, and relative RDC accuracy is critical to proper weighting of different RDC types in refinement calculations. It is of particular interest

*To whom correspondence should be addressed. E-mail: rabyrd@ncifcrf.gov

to measure couplings outside the peptide plane since the planar peptide bond renders certain dipolar couplings interdependent (Mueller et al., 2000).

Two methodologies predominate RDC measurement. The first method relies on measuring frequency displacements, and it is therefore limited to well resolved spectra, since the number of resonances is doubled. The resonance overlap problem is often exacerbated in proteins for couplings involving C^{α} resonances due to inherently poor chemical shift dispersion, rapidly making this method less applicable as molecular size increases. Recording different components of the J-coupled multiplet in separate spectra helps combat spectral crowding, though doubles the experiment time (Ross et al., 1996; Meissner et al., 1997; Ottiger et al., 1998). Extension to a third frequency dimension lessens spectral crowding; however, experiment time is significantly increased and poor digitization in the indirect dimensions severely limits measurement precision, especially for smaller couplings (Tjandra and Bax, 1997a; Yang et al., 1998; Permi, 2003).

The second method is quantitative J-modulation, which encodes the coupling of interest into an intensity modulation of a correlated resonance peak. Advantages of this approach include reduction in spectral complexity, removal of lineshape fitting artifacts, and straightforward analysis of experimental error. This method was first applied to H^{N}–N and H^{α}–C^{α} couplings recorded in intensity modulated ^{15}N- and ^{13}C-HSQCs, respectively (Tjandra et al., 1996; Tjandra and Bax, 1997b). Similar to the frequency displacement methods, application of J-modulation is often restricted to well resolved spectra, again making $^{1}H^{\alpha}$–$^{13}C^{\alpha}$ correlated spectra of limited use. Addition of a third frequency dimension does not suffer the same digitization limitation as 2D-IPAP experiments, however, the additional experiment time required drastically decreases the number of intensity-modulated spectra that can be obtained in a reasonable amount of time, again limiting measurement accuracy and precision (Chou et al., 2001).

Generally, $^{1}H^{N}$–^{15}N correlation resonances in most proteins are much better resolved than $^{1}H^{\alpha}$–$^{13}C^{\alpha}$ resonances. Since all backbone resonances can be correlated to the intra- or inter-residue H^{N}–N resonances, it is reasonable to encode couplings associated with backbone atoms into a familiar 2D H^{N}–N correlation spectrum. This can be achieved by modulating the detected H^{N}–N resonance intensity by a backbone coupling of interest. Taking a series of spectra in which the coupling is allowed to evolve for different amounts of time allows the coupling to be measured. In this way, more backbone couplings can be measured with greater speed, accuracy, and precision than before.

To date, two strategies have explored this idea. The first employs out-and-back HNCO or HN(CO)CA magnetization transfers with a delay-inversion-delay block for intensity modulation (Evenas et al., 2001; Mittermaier and Kay, 2001). Stepwise variation of the two symmetric delays results in magnetization amplitude modulated by an exponentially damped sinusoid requiring multiple variables for data fitting and more complex error analysis. A second strategy utilizes constant time J-modulation to measure H^{α}–C^{α} couplings (Hitchens et al., 1999). Magnetization is sinusoidally modulated providing the advantage of single parameter data fitting and readily calculable experimental error. However, in that experiment, long periods of transverse $^{13}C^{\alpha}$ magnetization limit sensitivity, especially for larger proteins.

In this report, we present a suite of experiments that takes advantage of $^{1}H^{N}$ and ^{15}N chemical shift dispersion to measure H^{α}–C^{α}, C^{α}–C', C^{α}–C^{β}, and H^{N}–N couplings in a series of two-dimensional intensity modulated $^{1}H^{N}$–^{15}N correlation spectra. Valuable couplings can be obtained without H^{α} assignments or in cases where side-chain assignments are incomplete. Experimental sensitivities are lower than a typical ^{15}N-HSQC, but constant-time ^{15}N chemical shift evolution enables a compromise of greater signal averaging on fewer indirect increments combined with linear prediction to achieve the same resolution. Single parameter data fitting and simplified error analysis are additional benefits of using these experiments. We demonstrate this suite of measurements on ubiquitin in isotropic and sterically aligned conditions. Also, isotropic data for 16 kDa Interleukin-4 (IL-4) and 18 kDa NusB were collected to demonstrate the applicability of these experiments to larger proteins. The entire suite of experiments can be slightly modified to incorporate $^{13}C'$ evolution instead of ^{15}N evolu-

tion, thereby retaining the simple two-dimensional spectra and data analyses while resolving more resonances in larger proteins or proteins with extensive overlap in the ^{1}H–^{15}N–HSQC spectra (Caffrey et al., 1998).

Materials and methods

Protein samples

Isotropic data were collected from a 1 mM uniformly ^{15}N, ^{13}C labeled sample of ubiquitin in 20 mM sodium acetate, pH = 4.7 and 10 μM NaN_3. Aligned data were collected under the same buffer conditions with 600 μM protein in a stretched 5.8% polyacrylamide gel (Tycko et al., 2000; Sass et al., 2000; Chou et al., 2001). Isotropic IL-4 J-couplings were measured from a 600 μM sample in 20 mM $NaHPO_4$, pH = 6.1, 50 mM NaCl, 100 μM EDTA, and 10 μM NaN_3. Isotropic data for NusB was collected from a 700 μM sample in 50 mM $NaPO_4$, 200 mM NaCl, pH = 6.5.

Data collection and processing

All data were collected at 25 °C on 500, 600, and 800 MHz Varian Inova spectrometers. All spectrometers were equipped with *z*-gradient cryogenic probes. J-modulated spectra were collected in an interleaved fashion using the pulse sequences shown in Figures 1–3. Pseudo-3D spectra were separated into 2D sub-spectra subsequent to identical processing utilizing NMRPipe

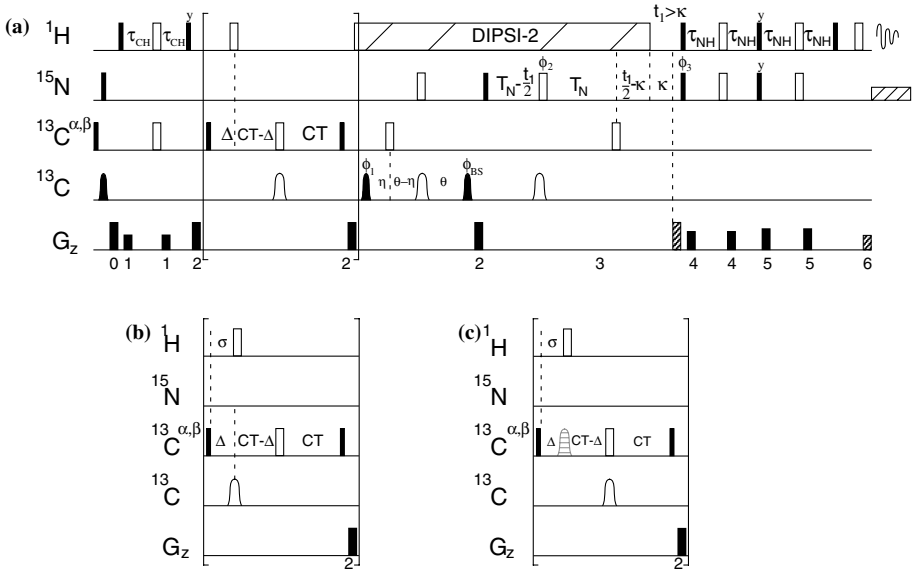

Figure 1. Pulse sequences (a) HN(J-HACA), (b) HN(J-CACO), and (c) HN(J-CACB) used to measure H^{α}–C^{α}, C^{α}–C' and C^{α}–C^{β} RDCs, respectively. Filled (outlined) shapes represent pulses applied with a flip angle of 90° (180°). Pulses are of x-phase, unless indicated otherwise. ϕ_{BS} is a Bloch–Siegert compensation phase, typically less than 10°. The ^{1}H, ^{13}C, and ^{15}N carriers are positioned at 4.7 (water), 46, and 115.5 ppm, respectively. All ^{1}H (^{15}N) pulses are applied at a field strength of 36 (5.8) kHz. Rectangular $^{13}C^{\alpha}$ pulses are selective square pulses applied at a field strength of $d/\sqrt{15}$ (90°) or $d/\sqrt{3}$ (180°) where d is the separation in Hz between the centers of the $^{13}C'$ and $^{13}C^{\alpha}$ chemical shift regions (Geen and Freeman, 1991). All $^{13}C'$ pulses are shifted square selective pulses of the same pulse width as their C^{α} counterparts. Shaped pulses may be substituted for these selective rectangular pulses with the potential for a modest (ca. 10%) improvement in sensitivity. In (c), the horizontally dashed C^{β} inversion pulse is a shaped g3 pulse of width 750 μs, centered at 26 ppm (Emsley and Bodenhausen, 1990). The delays used are $\tau_{CH} = 1.7$ ms, $\tau_{NH} = 2.4$ ms, Δ is incremented (see text), CT = 14.2 ms, $\eta = 4.6$ ms, $\theta = 14.0$ ms, $T_N = 14.0$ ms, $\kappa = 5.4$ ms, and $\sigma = 1.7$ ms. The phase cycling employed is $\phi_1 = x, -x$; $\phi_2 = x, x, y, y, -x, -x, -y, -y$; $\phi_3 = x, -x$; and rec = $2(x, -x, -x, x)$. Quadrature detection in F_1 is achieved by using the gradient-enhanced sensitivity method in which two separate data sets are recorded for each t_1 increment with 180° added to ϕ_3 and the sign of gradient 3 inverted for the second set (Kay et al., 1992; Schleucher, 1993). The gradients used are $g_0 = 0.5$ ms, 8 G/cm; $g_1 = 0.75$ ms, 27 G/cm; $g_2 = 0.25$ ms, 41 G/cm; $g_3 = 2.5$ ms, 27 G/cm; $g_4 = 0.5$ ms, 16 G/cm; $g_5 = 0.5$ ms, 6 G/cm; $g_6 = 0.25$ ms, 27 G/cm. Experiments are shown without TROSY enabled for simplicity.

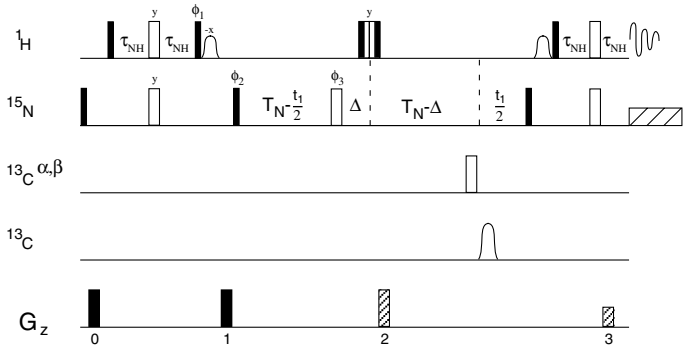

Figure 2. HN(J-HN) pulse sequence. All notation and parameter values are the same as for the HN(J-HACA) sequence in Figure 1a unless noted. The ^{13}C carrier is positioned at 56 ppm and the ^{1}H inversion pulse during the J-modulation block is of the composite variety. The delays are $\tau_{NH} = 2.5$ ms and $T_N = 16.7$ ms. Water selective flip-back pulses were shaped 1.7 ms sinc pulses. The phase cycling employed is $\phi_1 = y, -y$; $\phi_2 = \{2(x), 2(y), 2(-x), 2(-y)\}$ or $\{2(x), 2(-y), 2(-x), 2(y)\}$; $\phi_3 = 8(x), 8(y), 8(-x), 8(y)$; and rec = $x, -x, y, -y, 2(-y, y, -x, x), x, -x, y, -y$. The gradients used are $g_0 = 1.0$ ms, 41 G/cm; $g_1 = 2.0$ ms, 33 G/cm; $g_2 = 2.5$ ms, 27 G/cm; $g_3 = 0.25$ ms, 27 G/cm. As before, quadrature detection is achieved by selecting the appropriate ϕ_2 phase cycle and sign of g_2.

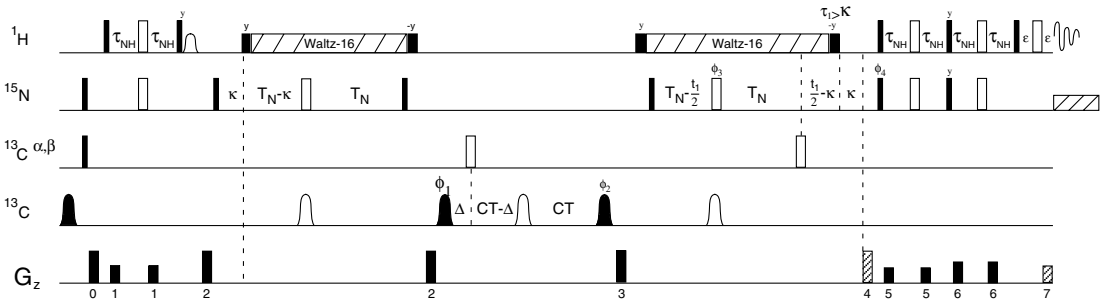

Figure 3. Out-and-back HN(J-COCA) pulse sequence. All notation and parameter values are the same as for the HN(J-HACA) sequence in Figure 1a unless noted. The ^{13}C carrier is positioned at 174 ppm, CT was set to 28.4 ms, and the additional ε delays were approximately 360 μs. All on resonance C′ pulses are of the sinc variety and $C^{\alpha,\beta}$ inversion pulses are shifted square selective pulses. The water selective flip-back pulse was a shaped 1.7 ms sinc pulse. The phase cycling employed is $\phi_1 = x, -x$; $\phi_2 = 2(x), 2(-x)$; $\phi_3 = 4(x), 4(-x)$; $\phi_4 = x, -x$; and rec = $x, 2(-x), x$. The gradients used are $g_0 = 1.0$ ms, 20 G/cm; $g_1 = 0.5$ ms, 16 G/cm; $g_2 = 1.0$ ms, 22 G/cm; $g_3 = 1.0$ ms, 16 G/cm; $g_4 = 2.5$ ms, 27 G/cm; $g_5 = 0.5$ ms, 4 G/cm; $g_6 = 0.5$ ms, 6 G/cm; $g_7 = 0.25$ ms, 27 G/cm. Quadrature detection is achieved by inverting ϕ_4 and g_4.

(Delaglio et al., 1995). Typical parameters included 8–32 scans per fid, 1024 complex points in the ^{1}H acquisition dimension, and 34 complex points in the indirect ^{15}N dimension, resulting in acquisition times of 30–120 min per 2D correlation spectrum. The total measurement duration is dependent on the number of sampling points (see below). The indirect dimension was mirror image linear predicted to four times the original data size and Gaussian window functions were applied in both dimensions prior to zero-filling. Peak volumes were determined by fitting the lineshapes to two-dimensional Gaussians and calculating the volume using tools within NMRPipe. The resulting peak volumes were plotted and fit to the appropriate equation in Table 1 using the nlinLS and modelXY tools present within NMRPipe. Monte Carlo simulations were used to estimate error implementing a one standard deviation confidence interval. These procedures are similar to standard analyses of relaxation data using NMRPipe. The principal axis system (PAS) for alignment of ubiquitin was calculated from the measured RDCs using the programs

Table 1. Modulation equations and symmetry points

Experiment	Amplitude modulation	Symmetry point
HN(J-HACA)	$I_o \sin(2\pi J_{H^\alpha C^\alpha} \Delta)$	0
HN(J-CACO)	$I_o \sin(2\pi J_{C^\alpha C'} \Delta)$	0
HN(J-COCA)	$I_o \cos(2\pi J_{C^\alpha C'} \Delta)$	0
HN(J-CACB)	$I_o \cos(2\pi J_{C^\alpha C^\beta} (\Delta - CT))$	CT
HN(J-HN)	$I_o \cos(2\pi J_{H^N N} (CT - \Delta))$	T_N

Orderten-SVD and REDCAT (Losonczi et al., 1999; Valafar and Prestegard, 2004). Theoretical RDCs were calculated from the coordinates of the solution structure of ubiquitin (PDB accession 1D3Z (Cornilescu et al., 1998)) oriented in the PAS. In all comparisons of calculated *versus* observed RDCs, the structure was not refined against the RDCs measured in this work. IPAP spectra were collected with 16 scans per fid, 1024 complex points in the ^{1}H acquisition dimension, and 200 complex points in the indirect ^{15}N dimension. Gaussian window functions were applied to both dimensions before zero-filling, with the indirect dimension being zero-filled to 512 points prior to Fourier Transformation. Peaks were fit analogously to J-modulated data and peak centers in both dimensions were determined from the Gaussian fit.

Pulse sequence description

A suite of experiments has been designed to modulate the intensity of an H^N–N crosspeak by one of the desired couplings. First, we consider a pulse sequence for measuring H^α–C^α couplings, HN(J-HACA), shown in Figure 1a. The magnetization transfer is as follows:

$$H^\alpha{}_{(i-1)} \rightarrow C^\alpha{}_{(i-1)}\{\sin(2\pi J_{H^\alpha C^\alpha}\Delta)\} \rightarrow C'{}_{(i-1)} \rightarrow N_{(i)}(t_1) \rightarrow H^N{}_{(i)}(t_2)$$

Amplitude modulation is achieved during the J-modulation block delimited by brackets in figure 1a. Details of this pulse sequence element are analogous to a semi-constant time period, which has been discussed in detail elsewhere (Grzesiek and Bax, 1993). Briefly, H^α–C^α couplings are active for a time Δ, followed by refocusing for a time CT−Δ, and are active again for a time CT, resulting in a total coupling evolution of 2Δ. Focusing only on H^α and C^α, magnetization evolving from anti-phase $H^\alpha C^\alpha$ to in-phase C^α is selected at the end of the J-modulation block and transferred to C′, thereby alleviating the need to refocus H^α and resulting in $\sin(2\pi J_{H^\alpha C^\alpha}\Delta)$ amplitude modulation (see Table 1). Sensitivity losses due to fast transverse C^α and C′ relaxation were reduced by minimizing the duration of C^α transverse magnetization and taking advantage of $1/2J_{C^\alpha C^\beta} \approx 3/4J_{C^\alpha C'}$, which permitted combining the C^αC′ INEPT into the J-modulation block by addition of a single carbonyl inversion pulse. These modifications account for improved sensitivity compared to an earlier experiment (Hitchens et al., 1999). The ^{1}H carrier was left on resonance for water and signal loss from off-resonance effects during ^{1}H decoupling, which can become appreciable at high fields, was observed to be insignificant for well calibrated decoupling. ^{15}N chemical shift is evolved in a constant-time manner during t_1 and the Rance–Kay PEP-sensitivity enhancement with gradient selection precedes acquisition (Cavanagh and Rance, 1990; Kay et al., 1992). To allow for data mirroring, the initial zero crossing (i.e. when $\Delta = 0$) was carefully calibrated by introducing a small, adjustable delay to compensate for finite pulse effects.

Exchanging the bracketed block in Figure 1a with that shown in Figure 1b allows for selection of C^α–C′ couplings using the HN(J-CACO) pulse sequence. In contrast to the HN(J-HACA) experiment, a fixed $1/4J_{H^\alpha C^\alpha}$ delay (σ) is introduced before the ^{1}H inversion so that H^α magnetization is refocused before decoupling is initiated to yield in-phase C^α magnetization at the end of the J-modulation block. Also, the C′ inversion pulse is incremented by Δ through the J-modulation block instead of a ^{1}H inversion pulse. Since the anti-phase C^αC′ scalar coupling component is selected, magnetization is again sine modulated and data is handled the same as for the HN (J-HACA) experiment.

Exchanging the bracketed block in Figure 1a with that shown in Figure 1c allows for selection of C^α–C^β couplings via the HN(J-CACB) pulse sequence. Similar to the HN(J-CACO) experiment, H^α is refocused during the J-modulation block before ^{1}H decoupling begins. Introduction of a selective C^β inversion pulse at the end of the first Δ delay is responsible for intensity modulation. Since the in-phase C^α term is selected instead of the anti-phase $C^\alpha C^\beta$ term,

magnetization is cosine modulated. Another subtle difference from the HN(J-CACO) pulse sequence is the evolution of scalar coupling during the J-modulation block. Since the semi-selective square C^{α} pulse inverts both C^{α} and C^{β} resonances, scalar coupling evolves for the time Δ, refocuses for the time CT$-\Delta$, and continues to refocus for the final CT period. The total coupling time is $2\Delta-2$CT, in which 2CT is a constant. Amplitude modulation is thus symmetric about CT, and therefore must be considered when arraying Δ such that points are collected at time of CT$-\Delta_o$, CT$-2\Delta_o$, CT$-3\Delta_o$, etc., where Δ_o is the optimal sampling increment defined below. Also, data must be mirrored about the point of symmetry CT, instead of zero. If not handled properly during data mirroring, significant error can be introduced into the measured couplings.

The selective C^{β} inversion pulse in the J-modulation block is critical to the experiment. If this pulse nutates a C^{α} resonance, improper modulation will be observed for the corresponding residue. If the C^{β} pulse does not completely invert C^{β} resonances, accurate coupling values cannot be extracted from the resulting data. A *g*3 inversion pulse (Emsley and Bodenhausen, 1990) with a width of 44 ppm, centered at 24 ppm was used. Fortunately, since glycine residues do not have C^{β}s, their roughly 46 ppm C^{α} resonances can be ignored providing a larger window for the leading edge of the pulse. Since serine and threonine residues have C^{β} chemical shifts (typically 60–70 ppm) in the normal C^{α} range, they do not yield intensity-modulated peaks because they are not selectively inverted. Consequently, this experiment is able to measure C^{α}–C^{β} couplings for all residues except serines, threonines, glycines, and those preceding prolines.

To complete the suite, a J-modulated experiment to measure H^{N}-N couplings, HN(J-HN), similar to a previously published experiment (Tolman and Prestegard, 1996), is shown in Figure 2. It has the same framework as a standard, constant-time ^{15}N-HSQC except J-modulation has been introduced into the constant-time ^{15}N evolution period by replacing ^{1}H decoupling by a composite ^{1}H 180° pulse following a variable delay. As a result, a three-spin $H^{N}NC'$ state is created and mandates that the C′ inversion pulse, typically applied simultaneous with the ^{15}N inversion pulse, be moved to the end of the second constant-time period. Similar to the HN(J-CACB) experiment, the scalar coupling modulated in-phase term is selected resulting in the cosine modulation shown in Table 1. Furthermore, the order of the J-modulation block differs from that of the previous sequences in that the scalar coupling is active for $T_N - t_1$, refocused for Δ, and active again for $T_N + t_1$. The sum becomes $2T_N - 2\Delta$ and data incrementation and mirroring should be handled as described for the HN(J-CACB) experiment. This J-modulated experiment is effective for protonated and deuterated proteins and TROSY detection is an option for larger proteins.

An out-and-back version of the $C^{\alpha}C'$ experiment, referred to as the HN(J-COCA) pulse sequence, is shown in Figure 3. This experiment is useful for perdeuterated proteins. Magnetization transfer is as follows:

$$H^{N}_{(i)} \rightarrow N_{(i)} \rightarrow C'_{(i-1)}\{\cos(2\pi J_{C^{\alpha}C'}\Delta)\} \rightarrow N_{(i)}(t_1) \rightarrow H^{N}_{(i)}(t_2).$$

This experiment has a standard HNCO framework in which C′ chemical shift evolution has been replaced with a $C^{\alpha}C'$ J-modulation block. The first κ delay refocuses anti-phase $H^{N}N$ magnetization whereas the second κ delay generates anti-phase $H^{N}N$ magnetization prior to sensitivity enhancement and detection. As before, cosine modulation results from selecting the in-phase scalar coupling term instead of the anti-phase term and, analogous to the HN(J-HACA) experiment, data is mirrored about zero. However, since the magnetization amplitude is cosine modulated instead of sine modulated, no sign change is introduced during data mirroring. The out-and-back version of the experiment has greater sensitivity than the straight-through version, since no transfers utilizing fast relaxing transverse $^{13}C^{\alpha}$ magnetization are present. Improved sensitivity allows the CT period to be doubled and still have roughly a factor of two increase in sensitivity for ubiquitin over the straight-through experiment. The longer CT period is beneficial since more accurate and precise C^{α}–C′ couplings can be measured from Δ values spanning a greater period of time.

Results and discussion

Figures 1, 2 and 3 show the pulse sequences used to measure H^{α}–C^{α}, C^{α}–C^{β}, C^{α}–C′, and H^{N}–N

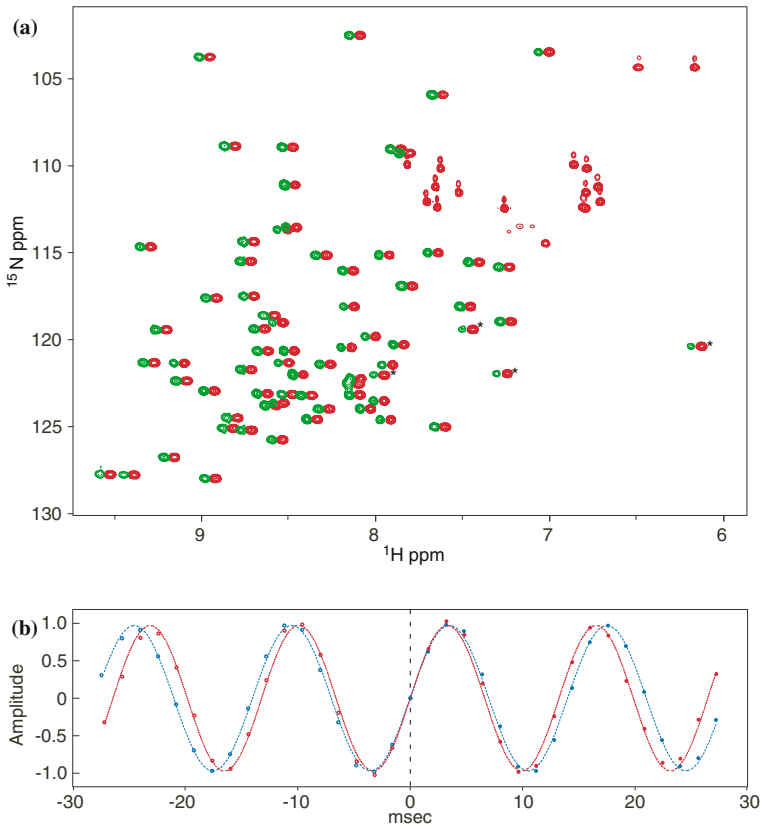

Figure 4. (a) Overlay of an ^{15}N-HSQC (red) and HN(J-HACA) (green) spectra taken from ubiquitin. A downfield ^{1}H shift of 0.06 ppm is imparted on the HN(J-HACA) spectra for clarity. The Δ delay in the J-modulated spectra was set to approximately $J_{H\alpha C\alpha}/4$, yielding an intensity maxima. Both spectra were acquired at 500 MHz in approximately 1 h. Resonances with an ∗ near the upper right follow glycines in the amino acid sequence. (b) Plot of HN(J-HACA) resonance intensity *versus* coupling evolution delay (2Δ). Isotropic intensities are shown in red whereas aligned intensities are shown in blue. Values were measured to be 142.77 ± 0.21 Hz for the isotropic coupling and 151.29 ± 0.04 Hz for the aligned coupling shown. Error bars for the fit intensities are subsumed in the circular symbols. The vertical dashed line indicates the point of symmetry, in this case 0. Acquired data is shown to the right in bold whereas mirrored data is shown to the left.

RDCs from a series of intensity modulated 2D ^{1}H–^{15}N correlation spectra. Intensity modulation is achieved during a constant time J-modulation block by incrementing the delay Δ. Couplings can be extracted on a per residue basis from plots of peak volume *versus* total coupling evolution time, 2Δ. An overlay of an ^{15}N-HSQC and HN(J-HACA) spectrum is shown in Figure 4. All resonances present in the HSQC are accounted for in the J-modulated spectra with the exception of side-chain NH_2 resonances. As expected, peak amplitudes for residues following glycine in the amino-acid sequence are diminished in the J-modulated spectra as a result of poor $H^{\alpha}C^{\alpha}$ INEPT transfer stemming from the presence of two glycine H^{α} atoms that effectively double the scalar coupling, causing a near null for the transfer.

Optimal sampling and data mirroring

In order to propose general methods for use with the suite of experiments, different strategies were compared to determine optimal sampling parameters. Initially, what will be called ‘true’ couplings were derived from a densely sampled data set in which more than 30 points per modulation period were collected. Various subsets of the densely sampled data were subsequently used to simulate different sampling strategies and to calculate couplings for comparison. As expected, regardless of the pattern of incrementation, sampling over a

larger range of Δ values produced more accurate couplings. Clustering data points around maxima and minima showed a slight improvement over clustering points around zero crossings, presumably due to the diminished effect of spectral noise on observed peak volumes. Mixing clusters around extrema with clusters around zero crossings had no significant effect. However, given a set number of points, linear sampling produced couplings closest to the true value with the least amount of error. It was empirically determined that approximately 8–10 points per period produced couplings identical (to within several hundredths of a Hz) to the 'true' values. This sampling criteria corresponds to optimal Δ increments (Δ_o) of roughly 0.8, 1.1, 2.0 and 3.0 ms for H^{α}–C^{α}, H^{N}–N, C^{α}–C′ and C^{α}–C^{β} couplings, respectively. Thus, as many data points as experiment time allows should be collected, incrementing from the point of symmetry in steps of no greater than Δ_o.

The number of Δ data points collected can be effectively doubled by taking advantage of the symmetric properties of sinusoidal functions and mirroring the data about the point of symmetry. During J-modulation, the order of evolution and selection of in-phase or antiphase coupling component determines the functional form of the amplitude modulation and the point of symmetry. The appropriate modulation function and symmetry point is listed in Table 1 for each of the J-modulated experiments presented. Data from cosine functions can simply be mirrored about the point of symmetry since $\cos(\Delta) = \cos(-\Delta)$. Sine functions have to include a sign change since $\sin(\Delta) = -\sin(-\Delta)$. When data mirroring was implemented (Figure 4b), improvements in calculated *versus* observed correlations were observed for all couplings measured. The greatest improvement, a 20% increase in R^2, was seen for C^{α}–C^{β} couplings. This is not surprising since only one half of a period could be sampled in the $1/2J_{C^{\alpha}C^{\beta}}$ constant time period. Although each complete set of modulated 2D spectra for isotropic ubiquitin was collected in under 4.5 hours, most samples will require more signal averaging. Data mirroring reduces the number of required experimental data points needed to obtain a given precision by a factor of two. When S/N is at all limiting, i.e., for samples of lower concentration or larger proteins, collecting twice as many transients per experiment is of more benefit than collecting more data points. The decrease in experiment time from data mirroring is especially beneficial for aligned samples since they tend to be more dilute, suffer from decreased INEPT transfer efficiencies (due to greater variations in effective scalar couplings resulting from the RDC contribution), and may not be stable for long periods of time.

Experiment time can further be reduced for couplings that are sine modulated since at time zero, the amplitude is zero. This provides a 'free' zero point for the volume fitting when finite pulse widths are properly accounted for. The proper zero point can be determined from 1D spectra (collected with a small variable delay introduced in the second CT period) to within 200 μs, introducing a small error into the individual scalar couplings, but resulting in a less than 1% average difference in measured RDCs. The zero crossing can be determined to well within 20 μs by analyzing peak volumes from analogously collected 2D spectra. An uncertainty of 20 μs introduces an average percent error in the H^{α}–C^{α} RDC measurement of less than 0.2%, a small fraction (less than 1/20th) of the typical experimental error.

This time savings does not apply to cosine modulated couplings since normalization to one at time zero requires a zero point be taken. Zero point considerations also impact optimal Δ incrementation since sampling over the greatest time span minimizes error. Given a set number of points incremented by Δ_o, in order to maximize the sampled time span and thereby minimize error, cosine modulated increments should be collected at times of $\Delta = \Delta_o/2$, $3\Delta_o/2$, $5\Delta_o/2$, etc. Since sine modulation provides a free zero point, spectra should be collected at times Δ_o, $2\Delta_o$, $3\Delta_o$, etc.

Comparison of measured RDCs from ubiquitin

Part of the motivation for developing this suite of experiments was the conjoined use of multiple RDCs in structural problems, including the need for accurate measurement of small RDCs due to paramagnetic alignment (Gaponenko et al., 2002; C.A. Fowler, submitted). We illustrate the degree of self-consistency and errors involved with H^{α}–C^{α}, C^{α}–C′, C^{α}–C^{β} and H^{N}–N RDCs using

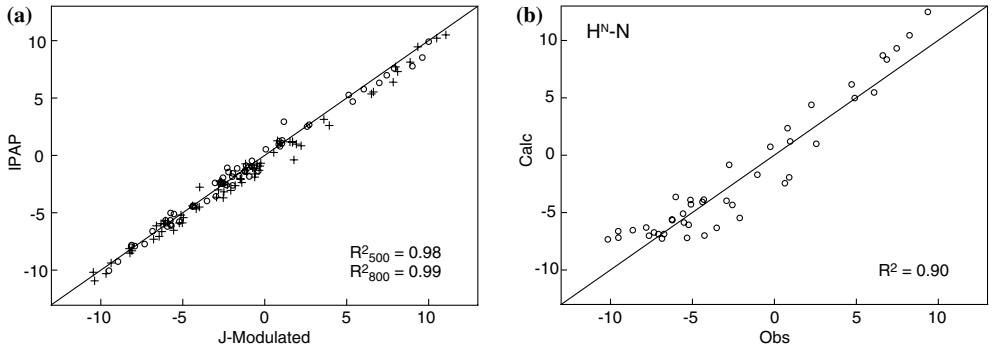

Figure 5. (a) Comparison of J-modulated and IPAP H^N–N RDCs. 500 MHz couplings are shown as circles whereas 800 MHz couplings are shown as plus signs. The black line shows $y = x$. J-modulated and IPAP RDCs were essentially identical with R^2 correlations of greater than 0.98. (b) Observed J-modulated H^N–N RDCs measured at 500 MHz are plotted *versus* calculated couplings. R^2 correlations are shown in the lower right.

Table 2. PAS parameters for ubiquitin

Coupling used	α (°)	β (°)	γ (°)	Da (Hz)	*R*	$^{HN}Da^a$
500 MHz						
HN(J-HACA)	144.2 ± 2.0	24.0 ± 0.7	97.2 ± 2.1	22.9 ± 2.2	0.49 ± 0.05	11.0 ± 1.1
HN(J-CACO)	143.3 ± 5.1	23.2 ± 2.0	94.7 ± 4.5	2.3 ± 0.6	0.43 ± 0.10	12.3 ± 3.0
HN(J-COCA)	143.9 ± 3.9	23.8 ± 1.2	96.7 ± 2.8	2.4 ± 0.5	0.46 ± 0.09	12.8 ± 2.5
HN(J-HN)	144.4 ± 2.4	23.6 ± 0.7	94.8 ± 2.3	−10.4 ± 0.8	0.49 ± 0.04	−10.4 ± 0.8
HN(J-CACB)[b]	142.0 ± 12.9	23.0 ± 2.8	102.0 ± 8.4	2.6 ± 0.9	0.34 ± 0.13	13.9 ± 5.0
Combined	144.5 ± 1.6	23.8 ± 0.6	96.3 ± 1.5	22.3[c] ± 1.7	0.49 ± 0.04	10.7 ± 0.8
800 MHz						
HN(J-HACA)	142.5 ± 1.7	24.4 ± 0.8	99.0 ± 1.8	23.1 ± 1.4	0.50 ± 0.03	11.1 ± 0.7
HN(J-COCA)	134.9 ± 6.1	23.2 ± 2.1	99.2 ± 4.6	2.5 ± 0.6	0.49 ± 0.12	13.4 ± 3.3
HN(J-HN)	144.8 ± 2.0	24.3 ± 0.5	95.4 ± 1.8	−11.3 ± 0.7	0.53 ± 0.03	−11.3 ± 0.7
Combined	143.5 ± 1.5	24.2 ± 0.5	97.5 ± 1.4	22.2[c] ± 1.2	0.51 ± 0.03	10.6 ± 0.6

[a]Normalized to HN.
[b]Data acquired at 600 MHz.
[c]Normalized to $H^{\alpha}C^{\alpha}$.

ubiquitin. First, H^N–N RDCs were measured using both an IPAP experiment (Ottiger et al., 1998) and the HN(J-HN) experiment. As shown in Figure 5a, IPAP and J-modulated H^N–N couplings are nearly identical. For data collected in the same amount of time, the standard deviation in the IPAP RDCs was ±0.06 Hz, essentially the same as the average ±0.07 Hz error determined from HN(J-HN) data without mirroring. With data mirroring, the average HN(J-HN) error for concentrated ubiquitin was reduced to ±0.04 Hz, well below those obtained using the IPAP method. HN(J-HN) errors could be further reduced by increasing experiment time, either from greater signal averaging or collecting more data points. The measured H^N–N RDCs fit the ubiquitin structure well (Figure 5b), having an R^2 correlation coefficient of 0.90 between calculated and observed RDCs. The resulting alignment tensor is the same as that determined for other measured RDCs (Table 2). Discrepancies between calculated and observed values can be attributed to structural noise (Zweckstetter and Bax, 2002), especially since the coordinates used were not refined against any of the RDCs measured in this work.

Though not as commonly measured as H^N–N RDCs, H^{α}–C^{α} RDCs are particularly useful

constraints for structural refinement since they are outside the peptide plane. Also, the magnitude of H^{α}–C^{α} RDCs is approximately 2.1 times larger than the magnitude of H^{N}–N RDCs making them more amenable to measurement in more weakly aligned samples. In addition to RDCs, isotropic H^{α}–C^{α} scalar couplings alone can be used to probe protein backbone conformations (Vuister et al., 1993; Edison et al., 1994). Using the HN(J-HACA) experiment in Figure 1a, H^{α}–C^{α} RDCs were measured for ubiquitin at 500 and 800 MHz. Data from both fields yielded identical tensors when fit to the known structure, and the RDC values at both fields agreed well for each residue. Figure 6a shows plots of calculated *versus* observed H^{α}–C^{α} couplings at 500 MHz. H^{α}–C^{α} RDCs were measured with an average error of ± 0.13 Hz in roughly 4.5 h for $J_{H^{\alpha}C^{\alpha}}$ and 16.5 h for $(J_{H^{\alpha}C^{\alpha}} + D_{H^{\alpha}C^{\alpha}})$.

C^{α}–C' RDCs are useful for constraining backbone orientations; however, since the couplings are relatively small, precise measurement is required. Compared to 3D methods, C^{α}–C' RDCs can be measured faster and with greater precision using the HN(J-CACO) and HN(J-COCA) sequences in Figures 1b and 3, respectively. For ubiquitin at 500 MHz, the sensitivity of the HN(J-COCA) experiment, with the doubled CT period, was nearly twice that of its straight-through counterpart HN(J-CACO). The increased sensitivity is predominantly due to the absence of magnetization transfers utilizing transverse $^{13}C^{\alpha}$ magnetization. With the added benefit of being applicable to perdeuterated proteins, the out-and-back HN(J-COCA) version is clearly superior for coupling measurements. To demonstrate the utility of this experiment, we measured isotropic $J_{C^{\alpha}C'}$ data for ubiquitin in 4.5 h and

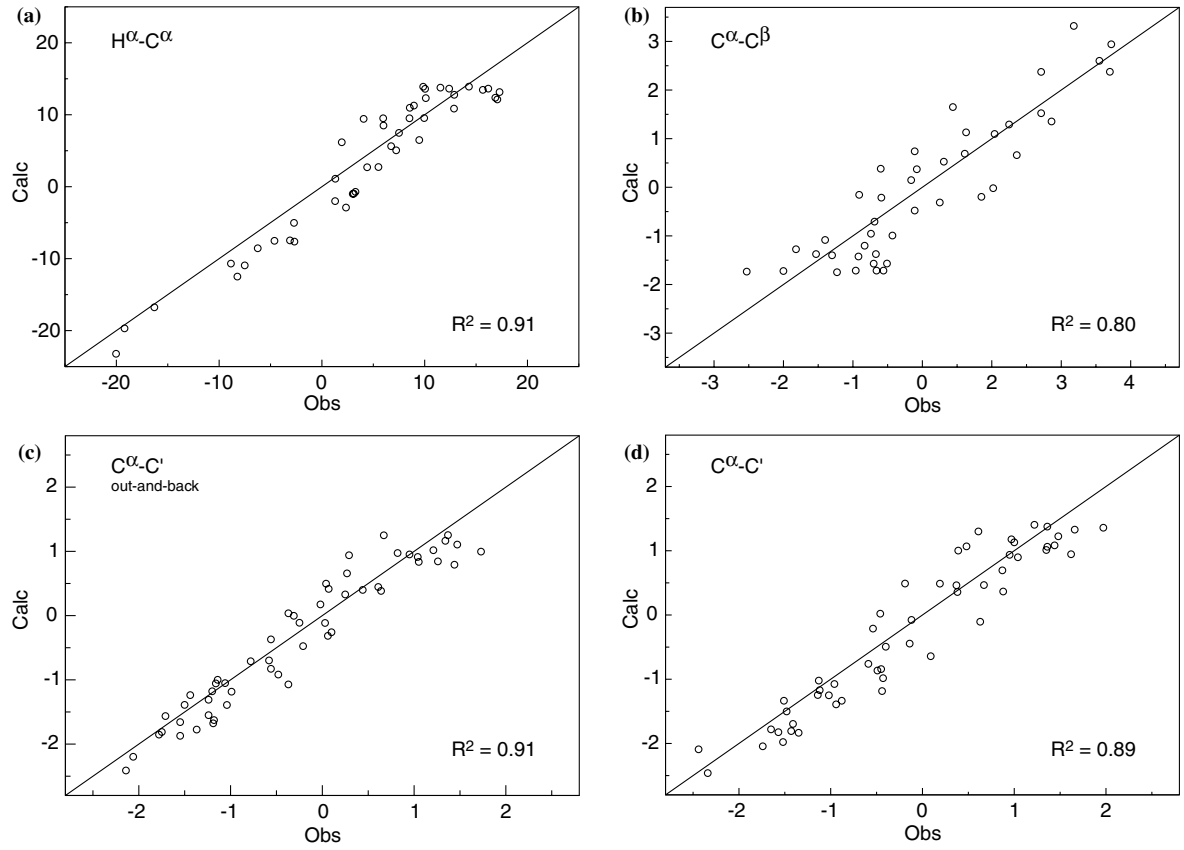

Figure 6. Calculated *versus* observed RDCs for ubiquitin. The black line represents $y = x$ and R^2 correlations are shown in the lower right. H^{α}–C^{α}, C^{α}–C^{β}, C^{α}–C'-ob, and C^{α}–C' couplings are shown in (a), (b), (c) and (d), respectively.

($J_{C^\alpha C'} + D_{C^\alpha C'}$) data in 16 hours. The C^α–C′ RDCs could be determined with an average error less than ± 0.05 (± 0.11) from the out-and-back (straight-through) experiment. Calculated *versus* observed data are shown in Figures 6c and d. C^α–C′ RDCs measured using both pulse sequences result in the same alignment tensor, identical to the alignment tensor determined from the other types of RDCs (see Table 2).

The C^α–C^β coupling is another RDC outside of the peptide plane that helps constrain the backbone dihedral angle ψ and provides information on side chain orientation (Evenas et al., 2001; Mittermaier and Kay, 2001). Although less sensitive than the other experiments in the suite, HN(J-CACB) allows measurement of C^α–C^β RDCs in a straightforward fashion. Since CT is set to $1/2J_{C^\alpha C^\beta} = 14.2$ ms, coupling evolution can only be measured for approximately half of a period, resulting in lower precision for measured couplings. Doubling the data size by mirroring provides a significant improvement, increasing calculated *versus* observed R^2 correlations by greater than 20%. RDCs observed after data mirroring are plotted *versus* their calculated counterparts in Figure 6b and a linear correlation with R^2 of 0.8 shows a good fit to the structure. The calculated *versus* observed R^2 correlation is lower for the C^α–C^β couplings, attributed to the 1D3Z structure not being refined with any side-chain RDCs. The Euler angles describing the PAS determined from C^α–C^β RDCs alone (Table 2) show they fit the same alignment tensor as all other couplings within error. Regrettably, serine and threonine C^α–C^β couplings are not observable since their C^β chemical shifts fall in the C^α region and cannot be selectively inverted. Nevertheless, 81% (44 of 54) of the possible C^α–C^β RDCs were measured for ubiquitin.

In addition to determining the alignment tensor for each set of couplings individually, we combined all four couplings (Clore et al., 1998) and obtained a tensor consistent with the individual tensors. The analysis was performed on data obtained at both 500 and 800 MHz, yielding equivalent tensors within experimental error (Table 2). The quality of the combined fit at 500 (800) MHz is demonstrated by the reduced error in Da from an average of 2.5 (1.6) Hz for the individual fits to 0.8 (0.6) Hz for the combined fits. Overall the consistency of the tensor parameters obtained demonstrates the utility and accuracy of the common data acquisition and extraction proposed in the suite of experiments.

Larger proteins

To demonstrate the applicability of the experiments to larger proteins, data was acquired for the 16 kDa IL-4 and 18 kDa NusB proteins at 500 and 600 MHz. IL-4 has a measured correlation time of 7.6 ns at 35° (Redfield et al., 1992) and NusB has an estimated correlation times of 8.9 and 8.6 ns at 25° and 35°, respectively (Altieri et al., 2000). As correlation times increase, the sensitivity of the J-modulated experiments will decrease due to more efficient ^{13}C T_2 relaxation. Nevertheless, for experiments of equal time, ^1H–^{15}N relative peak intensities for standard ^1H–^{15}N HSQC compared to HN(J-HACA) peak intensities were 1.0:0.25, 1.0:0.15, and 1.0:0.07 and 1.0:0.10 for ubiquitin, IL-4, NusB at 25°, and NusB at 35°, respectively. A similar comparison for the HN(J-HN) experiment relative to a standard ^1H–^{15}N HSQC yielded relative ratios of 1.0:0.73, 1.0:0.54, and 1.0:0.49 for ubiquitin, IL-4 and NusB, respectively, all at 25°.

J-modulated experiments can be affected by cross-correlated relaxation, which leads to differential intensity of the two multiplet components (Brutscher, 2000). The effect increases with both molecular size and magnetic field strength and will be manifested by an exponential decay of the J-modulated intensity, as a function of delay time Δ. The effect is negligible for small to medium sized proteins and becomes observable for proteins with a correlation time of approximately 20 ns. For example, J-modulated experiments for a protein with a correlation time of 20 ns measured at 800 MHz field strength will exhibit a decay on the order of 13% of the maximum amplitude. The robust fitting procedures in nlinLS and modelXY are impervious to such small effects. Even when a decay on the order of 30% is present (which would correspond to a 50 ns correlation time at 800 MHz), an error less than the experimental error (i.e., less than 0.07 Hz), is introduced in the derived coupling.

The experiments have been developed to include optional TROSY-methods to improve $^1H/^{15}N$ resolution. However, ^{13}C relaxation still

limits the overall size of proteins to which the straight-through experiments can be applied. We anticipate that these experiments will be most useful at 500 and 600 MHz; however application to small proteins at ultra-high fields is also clearly feasible. The HN(J-HN) and HN(J-COCA) experiments hold great promise for large perdeuterated proteins. These experiments can be complimented by H^N–C′ modulated versions of the same experiments, in which significantly more resonances can often be resolved in the 2D spectra, as was demonstrated for gp41 (Caffrey et al., 1998).

Conclusions

H^α–C^α, H^N–N, C^α–C′, and C^α–C^β couplings can be efficiently, accurately, and precisely measured using J-modulated experiments that encode couplings in the peak intensities of 2D H^N–N and H^N–C′ correlation spectra. Since H^N–N resonances are typically better resolved than H^α–C^α resonances in proteins, more H^α–C^α couplings can generally be measured from this suite of experiments than from frequency differences in ^{13}C-HSQC spectra. In addition, J-modulated experiments are impervious to field-dependent chemical shift perturbations, such as dynamic frequency shifts, that can complicate other measurements, particularly important for small couplings. Precision can surpass that of IPAP measurements and allows for straightforward error analysis. The experiments presented readily allow for the measurement of H^α–C^α and C^α–C^β RDCs, two valuable couplings outside the peptide plane. Moreover, these couplings can be determined without complete H^α or C^β assignments. Taken as a whole, the suite of experiments allows for a uniform means of data collection, data processing, and extraction of RDCs, thus expediting their use in structure calculations and refinements.

Acknowledgements

We thank Amanda Altieri (SBL/NCI) and Frank Delaglio (LCP/NIDDK) for useful discussions and Jess Li and Jennifer Hans (SBL/NCI) for protein preparation and laboratory support.

References

Altieri, A.S., Mazzulla, M.J., Horita, D.A., Coats, R.H., Wingfield, P.T., Das, A., Court, D.L. and Byrd, R.A. (2000) *Nat. Struct. Biol.*, **7**, 470–474.
Brutscher, B. (2000) *Concepts Magn. Reson.*, **12**, 207–229.
Caffrey, M., Kaufman, J., Stahl, S.J., Wingfield, P.T., Gronenborn, A.M. and Clore, G.M. (1998) *J. Magn. Reson.*, **135**, 368–372.
Cavanagh, J. and Rance, M. (1990) *J. Magn. Reson.*, **88**, 72–85.
Chou, J.J., Gaemers, S., Howder, B., Louis, J.M. and Bax, A. (2001) *J. Biomol. NMR*, **21**, 377–382.
Clore, G.M., Gronenborn, A.M. and Bax, A. (1998) *J. Magn. Reson.*, **133**, 216–221.
Cornilescu, G., Marquardt, J.L., Ottiger, M. and Bax, A. (1998) *J. Am. Chem. Soc.*, **120**, 6836–6837.
Delaglio, F., Grzesiek, S., Vuister, G.W., Zhu, G., Pfeifer, J. and Bax, A. (1995) *J. Biomol. NMR*, **6**, 277–293.
Edison, A.S., Markley, J.L. and Weinhold, F. (1994) *J. Biomol. NMR*, **4**, 519–542.
Emsley, L. and Bodenhausen, G. (1990) *Chem. Phys. Lett.*, **165**, 469–476.
Evenas, J., Mittermaier, A., Yang, D. and Kay, L.E. (2001) *J. Am. Chem. Soc.*, **123**, 2858–2864.
Fischer, W.F., Losonczi, J.A., L., W.J. and Prestegard, J.H. (1999) *Biochemistry*, **38**, 9013–9022.
Gaponenko, V., Altieri, A.S., Li, J. and Byrd, R.A. (2002) *J. Biomol. NMR*, **24**, 143–148.
Geen, H. and Freeman, R. (1991) *J. Magn. Reson.*, **93**, 93–141.
Goto, N.K., Skrynnikov, N.R., Dahlquist, F.W. and Kay, L.E. (2001) *J. Mol. Biol.*, **308**, 745–764.
Grzesiek, S. and Bax, A. (1993) *J. Biomol. NMR*, **3**, 185–204.
Hitchens, T.K., McCallum, S.A. and Rule, G.S. (1999) *J. Magn. Reson.*, **140**, 281–284.
Kay, L.E., Keifer, P. and Saarinen, T. (1992) *J. Am. Chem. Soc.*, **114**, 10663–10665.
Losonczi, J.A., Andrec, M., Fischer, M.W. and Prestegard, J.H. (1999) *J. Magn. Reson.*, **138**, 334–342.
Meissner, A., Duus, J.O. and Sorensen, O.W. (1997) *J. Biomol. NMR*, **10**, 89–94.
Mittermaier, A. and Kay, L.E. (2001) *J. Am. Chem. Soc.*, **123**, 6892–6903.
Mueller, G.A., Choy, W.Y., Yang, D., Forman-Kay, J.D., Venters, R.A. and Kay, L.E. (2000) *J. Mol. Biol.*, **300**, 197–212.
Ottiger, M., Delaglio, F. and Bax, A. (1998) *J. Magn. Reson.*, **131**, 373–378.
Permi (2003) *J. Biomol. NMR*, **27**, 341–349.
Peti, W., Meiler, J., Bruschweiler, R. and Griesinger, C. (2002) *J. Am. Chem. Soc.*, **124**, 5822–5833.
Redfield, C., Boyd, J., Smith, L.J., Smith, R.A. and Dobson, C.M. (1992) *Biochemistry*, **31**, 10431–10437.
Ross, A., Czisch, M. and Holak, T.A. (1996) *J. Magn. Reson. A*, **118**, 221–226.
Sass, H.J., Musco, G., Stahl, S.J., Wingfield, P.T. and Grzesiek, S. (2000) *J. Biomol. NMR*, **18**, 303–309.
Schleucher (1993) *Agnew. Chem., Int. Ed. Engl.*, **32**, 1489.
Tjandra, N. and Bax, A. (1997a) *J. Am. Chem. Soc.*, **119**, 9576–9577.
Tjandra, N. and Bax, A. (1997b) *J. Magn. Reson.*, **124**, 512–515.

Tjandra, N., Grzesiek, S. and Bax, A. (1996) *J. Am. Chem. Soc.*, **118**, 6264–6272.
Tjandra, N., Omichinski, J.G., Gronenborn, A.M., Clore, G.M. and Bax, A. (1997) *Nat. Struct. Biol.*, **4**, 732–738.
Tolman, J.R. and Prestegard, J.H. (1996) *J. Magn. Reson. Ser. B*, **112**, 245–252.
Tolman, J.R., Al-Hashimi, H.M., Kay, L.E. and Prestegard, J.H. (2001) *J. Am. Chem. Soc.*, **123**, 1416–1424.
Tolman, J.R., Flanagan, J.M., Kennedy, M.A. and Prestegard, J.H. (1995) *Proc. Nat. Acad. Sci. USA*, **92**, 9279–9283.
Tycko, R., B., F.J. and Ishii, Y. (2000) *J. Am. Chem. Soc.*, **122**, 9340–9341.
Valafar, H. and Prestegard, J.H. (2004) *J. Magn. Reson.*, **167**, 228–241.
Vuister, G.W., Yamazaki, T., Torchia, D.A. and Bax, A. (1993) *J. Biomol. NMR*, **3**, 297–306.
Yang, D., Tolman, J.R., Goto, N.K. and Kay, L.E. (1998) *J. Biomol. NMR*, **12**, 325–332.
Zweckstetter, M. and Bax, A. (2002) *J. Biomol. NMR*, **23**, 127–137.